ChemComm

All-Metal σ-Antiaromaticity in Dimeric Cluster Anion $\{[CuGe_9Mes]_2\}^{4-}$

Journal:	*ChemComm*
Manuscript ID	CC-COM-04-2020-002525.R1
Article Type:	Communication

COMMUNICATION

All-Metal σ-Antiaromaticity in Dimeric Cluster Anion $\{[CuGe_9Mes]_2\}^{4-}$

Received 00th January 20xx,
Accepted 00th January 20xx

DOI: 10.1039/x0xx00000x

Zi-Chuan Wang,†[a] Nikolay V. Tkachenko,†[b] Lei Qiao,[a] Eduard Matito,[c,d] Alvaro Muñoz-Castro,[e] Alexander I. Boldyrev*[b] and Zhong-Ming Sun*[a]

In this work, we report a dimeric cluster anion $\{[CuGe_9Mes]_2\}^{4-}$, which was isolated as the $[K(2,2,2\text{-crypt})]^+$ salt and characterized by single-crystal X-ray diffraction and ESI mass spectrum. The title cluster represents the first locally *σ*-antiaromatic compound in the solid state, as well as the first heteroatomic antiaromatic compound.

Aromaticity and antiaromaticity may be a pair of the most extensively studied concepts in chemistry field,[1] which can be demonstrated by over 189,800 articles involved the aromaticity or antiaromaticity in recent 10 years.[2] The concept of anti-aromaticity was proposed by Breslow in his pioneering paper in 1965, intending to describe destabilization of those compounds caused by 4n π-electron system.[3] In 2003, Wang et al. observed all-metal antiaromatic Al_4^{4-} rectangle in $Li_3Al_4^-$ anion by photoelectron spectroscopy.[4] It was the first time that the concept of antiaromaticity was expanded from organic compounds to metal clusters. Subsequently, a series of antiaromatic metal clusters has been studied in gas phase, such as π-antiaromatic $[Al_3H_3]^{2-}$,[5] and σ-antiaromatic anionic Li_3^- and neutral Li_4.[6] Besides the homoatomic cases mentioned above, the heteroatomic antiaromatic fragments were also investigated by both experimental and theoretical chemists. 1,3,2,4-diazadiboretiidine ($B_2N_2H_4$) was once considered to be antiaromatic because it is an isoelectronic system as cyclobutadiene (C_4H_4) which is recognized antiaromatic model compound. However, due to the electronegativity difference between boron and nitrogen atoms, the electrons could not be effectively delocalized.[7] Thus, the actual synthesized $B_2N_2H_4$ derivatives did not exhibit the antiaromatic properties as predicted before.[8] Although the research on the antiaromaticity of metal clusters has made great progress in theoretical chemistry, the corresponding products in the solid phase have hardly been verified so far, especially compared to the aromatic species.[9] Our group has been working on the synthesis of aromatic clusters.[10] In 2016, our group synthesized the first all-metal π-antiaromatic complex, $[Ln(\eta^4\text{-}Sb_4)_3]^{3-}$ (Ln = La, Ho, Y, Er, Lu) in the solid state. The strong interaction between lanthanide cation and three *cyclo*-Sb_4 plays an important role in the stabilization of the highly reactive antiaromatic Sb_4 units.[10c] In the current work, we report the first case of all-metal σ-antiaromaticity in a synthesized anionic metal cluster $\{[CuGe_9Mes]_2\}^{4-}$, in which the heteroatomic antiaromatic Cu_2Ge_2 unit is stabilized by multiple local σ-aromatic germanium clusters.

Compound $\{[CuGe_9Mes]_2\}^{4-}$ (**1**) crystalized in the form of $[K(2,2,2\text{-crypt})]_4\cdot\mathbf{1}\cdot(DMF)_3$ was isolated in the DMF solution of Zintl phase K_4Ge_9, mesityl-copper (CuMes), and 2,2,2-crypt(4,7,13,16,21,24-hexaoxa-1,10-diazabicyclo [8.8.8] hexacosane), possessing triclinic space group $P\bar{1}$ symmetry. As exhibited in Figure 1, the anion species can be viewed as a dimer of $[CuGe_9(Mes)]^{2-}$, where a Cu atom and a substituted Ge were located at the apexes of the bicapped square antiprism of $CuGe_9$ respectively. Capped copper atom and a germanium atom at the waist of cage from each subunit formed diamond structure that connected the two subunits. The $[Cu_2Ge_{18}(Mes)_2]^{4-}$ presented *pseudo*-C_{2h} symmetric structure with Cu_2Ge_2 diamond as symmetry plane. Compared to other similar 10-atomic *closo*-cluster cages such as $[Ge_9ZnPh]^{3-}$,[11a] $[Ge_9CuP^iPr_3]^{3-}$ [11b] or $[Ge_9Pd(PPh)_3]^{3-}$,[11c] the $[Cu_2Ge_{18}(Mes)_2]^{4-}$ has an enlarged and slightly corrugated skeleton. The Ge-Ge bond lengths within the squares adjacent to the Cu atoms (Ge6-Ge9 and Ge10-Ge13) range from 2.6854(6)- 2.7730(6), which differs not much than that of other similar species. However, the Ge-Ge contacts within the squares adjacent to Ge1 and Ge18 were elongated to the range of 2.8171(6)-3.337(0), which are much longer than any adjacent Ge-Ge distance in the reported Ge clusters, as well as the electron-deficient oxidation coupling Ge clusters, such as

[a] *School of Materials Science and Engineering, State Key Laboratory of Element-Organic Chemistry, Tianjin Key Lab for Rare Earth Materials and Applications, Nankai University, Tianjin 300350, China, E-mail: sunlab@nankai.edu.cn.*
[b] *Department of Chemistry and Biochemistry, Utah State University 0300 Old Main Hill, Logan, UT 84322-0300, USA, E-mail: a.i.boldyrev@usu.edu.*
[c] *Donostia International Physics Center (DIPC), 20080 Donostia, Euskadi, Spain.*
[d] *IKERBASQUE, Basque Foundation for Science, 48011 Bilbao, Euskadi, Spain.*
[e] *Grupo de Química Inorgánicay Materiales Moleculares, Facultad de Ingenieria, Universidad Autonoma de Chile, El Llano Subercaseaux 2801, Santiago, Chile.*
† These authors contributed equally.
Electronic Supplementary Information (ESI) available. See DOI: 10.1039/x0xx00000x

$_{\infty}[Ge_9]^{2-}$,[12a] $[Ge_9\text{-}Ge_9]^{6-}$,[12b] $[Ge_9{=}Ge_9{=}Ge_9]^{6-}$ [12c] and $[Ge_9{=}Ge_9{=}Ge_9{=}Ge_9]^{8-}$.[12d] This was probably caused by the electron-withdrawing effect of mesityl group together with the formation of Cu_2Ge_2 diamond.

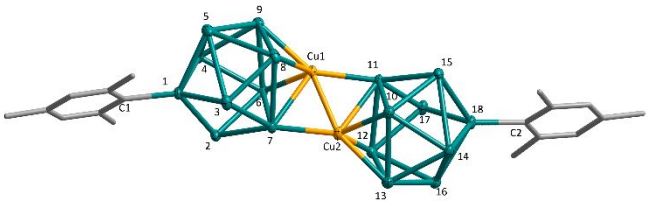

Figure 1. Structure of $\{[CuGe_9Mes]_2\}^{4-}$, thermal ellipsoids are drawn at the 50% probability level. Selected interatomic distances[Å]: Cu1-Cu2 2.5215(8), Cu1-Ge7 2.5998(7), Cu2-Ge7 2.4302(6), Cu1-Ge11 2.4007(6), Cu2-Ge11 2.6072(6), C1-Ge1 1.994(3), Ge8···Ge6 3.826(0), Ge2···Ge3 3.3769(0), Ge4-Ge5 2.8865(6), Ge2···Ge3 2.9867(0).

The averaged Cu-Ge bond length in **1** was 2.500(6), which was similar to that in functionalized germanium clusters such as $R_6Ge_{18}Cu$ (R = $Si(SiMe_3)_3$) (2.622 Å),[13a] $(Ge_9R_3)Cu(Ge_9R_3)CuPPh_3$ (2.571 Å),[13b] while longer than Ge-Cu σ-bond distance (2.362(1)) in $[Cu(\eta^4\text{-}Ge_9)(\eta^1\text{-}Ge_9)]^{7-}$.[11b] Interestingly, in the Cu_2Ge_2 diamond, the average length of Cu1-Ge7 and Cu2-Ge11 (2.6035(8)) are obviously longer than that of Cu2-Ge7 and Cu1-Ge11 (2.4154(6)), indicating that Cu seems to have stronger interaction with its opposite cluster than with its own subunit. This is identical to $\{[CuSn_5Sb_3]^{2-}\}_2$ where Cu atoms are also closer to the opposite cages.[14]

The formation of compound **1** is likely to derived from oxidation of K_4Ge_9 with excess 2 equiv. CuMes in the first step of the reaction, followed with nucleophilic substitution of Mes^- to generate $[Ge_9Mes]^{3-}$ species, which exhibited strong signal ($[K(2,2,2\text{-crypt})][Ge_9Mes]^-$, m/z=1188.61) in ESI-MS spectrum (Figure S4). Subsequently, $[Ge_9Mes]^{3-}$ assembled with copper cation, leading to the dimeric cluster. The signals of byproducts Ge_9Mes_2, $Ge_{18}Mes_2$ were also detected, suggesting that the $[Ge_9Mes]^{3-}$ species is relatively stable and its evolution to **1** is not the unique approach. Nevertheless, the formed compound **1** kept complete structure that showed a strong signal in mass spectrum (Figure 2). In our pretest study, reaction of K_4Ge_9 with 1 or 2 equiv. CuMes in ethylenediamine only yield copper mirror and amorphous germanium precipitate, suggesting that Cu^+ can effectively oxidize Ge_9 cluster but cannot be assembled into

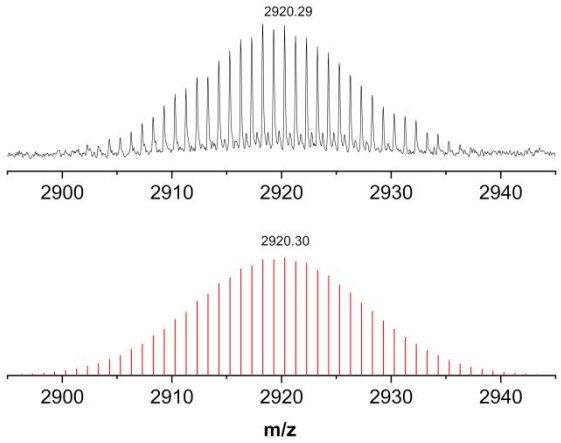

Figure 2. Negative-ion ESI mass spectrum of **1**. Measured (top) and simulated (bottom) spectrum of the fragment $[K(2,2,2\text{-crypt})]_3[Cu_2Ge_{18}Mes_2]^-$.

$$[Ge_9]^{4-} + 2CuMes \rightarrow [Ge_9]^{2-} + 2Cu + 2Mes^- \#(1)$$

$$[Ge_9]^{2-} + CuMes \rightarrow [Ge_9Mes]^{3-} + Cu^+ \rightarrow 1/2\,\{[CuGe_9Mes]_2\}^{4-} \quad (2)$$

Scheme 1. Possible mechanisms of the formation of **1**.

endohedral intermetalloid clusters like $[Cu@Sn_9]^{3-}$ and $[Cu@Pb_9]^{3-}$.[15]

Compared with η^4: η^1 coordinated $[Cu(\eta^4\text{-}Ge_9)(\eta^1\text{-}Ge_9)]^{7-}$,[11b] η^3: η^3 coordinated $(Ge_9R_3)Cu(Ge_9R_3)CuPPh_3$[13b] and face—fused $[Ge_{18}Pd_3(Sn^iPr_3)_6]^{2-}$,[13c] compound **1** represents a novel linkage manner for dimeric Zintl gemanium clusters. In order to understand the chemical bonding in $\{[CuGe_9Mes]_2\}^{4-}$ cluster, we firstly performed an Adaptive Natural Density Partioning (AdNDP)[6b,16] analysis of the monomeric $[CuGe_9Mes]^{2-}$ (**2**) specie. The optimized monomeric structure belongs to the C_s symmetry group while the metal cluster part is C_{4v}-symmetric and can be described as twice capped square antiprism (Figure 3). The 96 valence electrons of the whole structure were localized into 48 bonding elements, which could be divided into organic and metal cluster parts. The organic ligand consists of twenty 2-center 2-electron (2c-2e) C-C and C-H σ-bonds with occupation numbers (ONs) 1.99-1.97 |e|, and three 6c-2e π-aromatic bonds within the six-membered carbon ring (ON=1.99-1.96 |e|). The Mes ligand is bound to the Ge_9Cu cage via the 2c-2e Ge-C σ-bond with ON=1.96 |e| (Figure 3, b). The remaining 48 electrons are responsible for binding interactions inside the C_{4v}-symmetric metal cage. We found five classical Lewis d-type lone pairs on the Cu-atom (ON=1.99-1.96 |e|), eight s-type lone pairs on Ge-atoms (Figure 3, a), and eleven multicenter delocalized σ-bonds with ON=2.00-1.91 |e| (Figure 3, c-m). The latter eleven bonds responsible for the bonding inside of three areas in the Ge_9Cu cage. The first area, Ge_5 cap fragment, contains three 5c-2e σ-bonds with ON=1.97-1.90 |e| (Figure 3, c-e). Another area is $CuGe_4$ cap fragment with three 9c-2e σ-bonds (Figure 3, f-h). Although these bonds were found as 9-center, we should indicate them as $CuGe_4$ and not as $CuGe_8$ bonds, because of the large contribution of $CuGe_4$ fragment (~99-80%). The remaining five 9c-2e bonds (Figure 3, i-m) are responsible for binding of the Ge_8 antiprism (~99-97% contribution from germanium atoms). All three described fragments satisfy the Hückel electron counting rule and could be described as σ-aromatic. The complete bonding pattern of $[CuGe_9Mes]^{2-}$ could be found in the SI file (Figure S10). Notably, that the local σ-aromatic description of the $[CuGe_9Mes]^{2-}$ agrees with the previously discussed bonding in C_{4v}-$[Ge_9]^{4-}$ cluster, that possesses the same electron localization features and could be described with multiple local σ-aromatic fragments.[17]

Following the insights obtained from the monomeric species, we performed an AdNDP analysis of the novel dimeric C_{2h} $\{[CuGe_9Mes]_2\}^{4-}$ cluster (Figure S11). The optimized geometry is in good agreement with the experimental structure (Table S2). We found that the bonding pattern of $[CuGe_9Mes]^{2-}$ monomers in the dimeric cluster preserves almost the same. Each monomer consists of π-aromatic organic part bounded to the metal cage via Ge-C σ-bond,

twenty-four lone pairs on Cu and Ge atoms, and three locally σ-aromatic fragments inside the $CuGe_8$ cage. The main difference in bonding patterns of **1** and **2** hides in the number of germanium lone pairs. Only fourteen lone pairs were

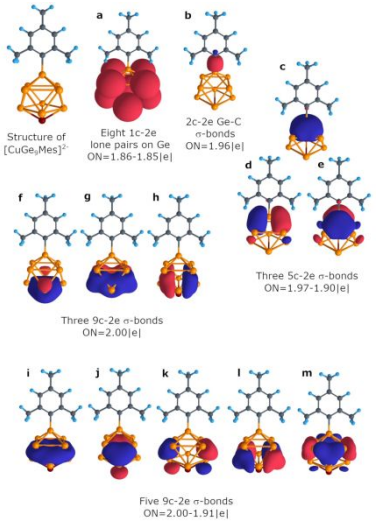

localized for **1**, while the remaining two germanium atoms in square antiprisms (Ge7 and Ge11) donate their four electrons (two electrons per each germanium) and form two 3c-2e σ-bonds (ON=1.92 |e|) responsible for binding of two monomers (Figure S18). The contribution of Ge atoms to these bonds is found to be ~84%. We note that those two bonds could also be found as 4c-2e with ON=1.93-1.92|e|. Thus, the

Figure 3. Chemical bonding picture of $CuGe_9$ fragment obtained for $[CuGe_9Mes]^{2-}$ cluster. ON denotes the occupation number (2.00 |e| in an ideal case). Lines between atoms help in visualization and do not necessarily represent 2c-2e bonds here and elsewhere.

interaction within the Cu_2Ge_2 diamond is the main difference between bonding pattern of monomer **2** and dimer **1**. The shape of the fragment, the chemical bonding picture, and the number of electrons (4e) render this interaction as antiaromatic. For previously investigated Li_4 σ-antiaromatic molecule, it was shown that the square geometry is unstable, and the global minimum structure is diamond shaped. Moreover, the antiaromaticity of Li_4 leads to the formation of locally 3c-2e σ-aromatic islands within the two Li_3 triangles.[6b] The same behavior is observed for Cu_2Ge_2 fragment. We want to note that the binding interactions between two monomers could also be described in terms of Wade-Mingos electron counting rules.[18] The detailed description could be found in the ESI file.

In order to furtherly prove the antiaromaticity of Cu_2Ge_2 fragment, we chose the most typical $NICS_{iso}$ and $NICS_{zz}$ indices[19] to perform analysis of special points at compound **1**. The highly positive $NICS_{zz}$ values agree with the antiaromatic description of the fragment. Moreover, the change of $NICS_{zz}$ with the distance from the center of the Cu_2Ge_2 fragment agrees nicely with the same results obtained for antiaromatic Li_4 cluster (Figure 4 and Table 1). The analysis of NICS for other points also confirms the σ-antiaromatic nature of compound points also confirms the σ-antiaromatic nature of compound **1** (Figure S12 and Table S4).

Figure 4. The $\{[CuGe_9Mes]_2\}^{4-}$ (a) and Li_4 (b) clusters with points that were selected for NICS indices calculations. Organic ligands are omitted for clarity.

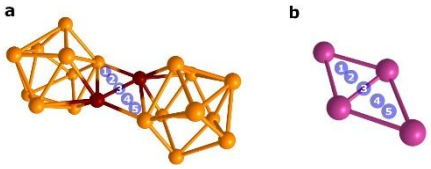

Table 1. $NICS_{iso}$ and $NICS_{zz}$ indices calculated for $\{[CuGe_9Mes]_2\}^{4-}$ and Li_4.

	$\{[CuGe_9Mes]_2\}^{4-}$		Li_4	
Point	$NICS_{iso}$	$NICS_{zz}$	$NICS_{iso}$	$NICS_{zz}$
1	-44.59	2.11	-5.33	-1.18
2	-24.83	14.52	0.88	5.16
3	-19.45	18.09	6.41	9.01
4	-24.83	14.52	0.88	5.16
5	-44.59	2.11	-5.33	-1.18

In Figure 5, the global magnetic behavior of the monomer and dimer are given in terms of an averaged and a specific orientation of the applied field, related to $NICS_{iso}$ (B^{ind}_{iso}) and to $NICS_{zz}$ (B^{ind}_{zz}). This support the aromatic behavior of the $CuGe_9$ cage, besides the mesityl group, in the monomer as denoted by the shielding region from B^{ind}_{iso}, and shielding cone behavior from different orientation for the former cage. Noteworthy, the formation of $\{[CuGe_9Mes]_2\}^{4-}$ cluster introduces strong changes as result of the antiaromatic character of the Cu_2Ge_2 fragment given by its pair of locally 3c-2e σ-aromatic islands. This generates a deshielding region above the central Cu_2Ge_2 diamond in the B^{ind}_{iso} representation, which is enhanced under a parallel field (B^{ind}_{z}), as distinctive for antiaromatic rings as accounted from $NICS_{zz}$. For *x*- and *y*-orientations, the aromatic character of the $CuGe_9$ cage contributes to the shielding response at Cu_2Ge_2, leading to a negative $NICS_{iso}$ index. The contour plot representation (Figure S16) exhibits a shielding (blue) region connecting Ge7 and Ge11 atoms in the central diamond, which does not involve Cu1 and Cu2, supporting that Cu_2Ge_2 is an overall antiaromatic section. From B^{ind}_{z}, the overall antiaromatic character in

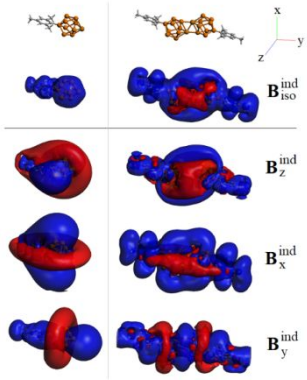

Cu_2Ge_2 is denoted resulting in a

Figure 5. Isosurface representation (±2 ppm) of the induced magnetic field, accounting for isotropic and specific orientation of the field. Blue: shielding; red, deshielding.

deshielding region compromising its four members, supporting the positive $NICS_{zz}$ values depicted above.

Finally, we have performed a topological analysis of the electron density of $\{[CuGe_9Mes]_2\}^{4-}$ cluster.[20] The isosurface

of the Laplacian (Figure S17) reveals a highly localized structure in the Cu_2Ge_2 moiety, which agrees with the antiaromatic character of this fragment. The most delocalized regions correspond to the π-aromatic rings of the organic ligand. The multicenter indices[21,22] confirm these results, giving a large I_{ring} value (0.036) for the π-aromatic ring and a small value (0.004) for Cu_2Ge_2. The latter value and the bond-order alternation (BOA=0.23) along the perimeter of the ring indicate that this moiety is antiaromatic. The topological analysis of the electron density (see the two ring critical points inside the Cu_2Ge_2 moiety in Figure S17) shows that Cu_2Ge_2 is composed of two ring structures (Cu-Ge-Cu). The latter exhibit positive I_{ring} values (0.04), indicating the 3c-2e nature of these interactions that was previously found by the AdNDP analysis. Conversely, neither the Laplacian of the electron density, nor the multicenter indices attribute a large aromatic character to the Ge_9Cu cage, although, the MCI value of the Ge_4Cu fragment (0.01) can be considered mildly aromatic.

In summary, the $[K(2,2,2\text{-crypt})]_4\{[CuGe_9Mes]_2\}(DMF)_3$ species was structurally characterized exposing the spontaneous formation of the dimeric $\{[CuGe_9Mes]_2\}^{4-}$ cluster avoiding oxidative coupling. The parent $[CuGe_9Mes]^{2-}$ monomer exhibits two aromatic motifs given by the organic mesityl-ligand and the deltahedral $CuGe_9$ cage. Interestingly, the dimer formation stands on a central σ-antiaromatic Cu_2Ge_2 diamond-like structure, involving two Cu_2Ge 3c-2e σ-aromatic islands. Such features enable the characterization of the first member for all-metal σ-antiaromatic species, as stable structural motif bringing together two organic-Zintl aromatic sides.

Conflicts of interest

There are no conflicts to declare.

Acknowledgements

This work was supported by the National Natural Science Foundation of China (No. 21971118, 21722106), the USA National Science Foundation (Grant CHE-1664379 to A. I. B). A.M.-C. funded by Fondecyt 1180683. E.M. acknowledges support from PGC2018-098212-B-C21 and EUR2019-103825 grants. The authors thank Prof. Slavi C. Sevov for valuable discussion and suggestions. The authors also thank the reviewers for comments on the discussion of Wade-Mingos rules.

Notes and references

1 a) J. C. Santos, W. Tiznado, R. Contreras and P. Fuentealba, *J. Chem. Phys.,* 2004, **120**, 1670; b) A. I. Boldyrev and L. S. Wang, *Chem. Rev.,* 2005**, 105**, 3716; c) M. Garcia-Borras, S. Osuna, J. M. Luis, M. Swart and M. Sola, *Chem. Soc. Rev.,* 2014, **43**, 5089; d) J. M. Mercero, A. I. Boldyrev, G. Merino and J. M. Ugalde, *Chem. Soc. Rev.,* **2015**, **44**, 6519; e) C. Liu, I. A. Popov, Z. Chen, A. I. Boldyrev and Z. M. Sun, *Chem. Eur. J.,* 2018, **24**, 14583.

2 This data is based on our search results by web of science on November 21th, 2019. For more details see Figure S15.

3 a) R. Breslow, *Chem. Eng. News.,* 1965, **43**, 90; b) R. Breslow, *Acc. Chem. Res.,* 1973, **6**, 393; c) M. D. Peeks, M. Jirasek, T. D. W. Claridge and H. L. Anderson, *Angew. Chem. Int. Ed.,* 2019, **58**, 15717.

4 A. E. Kuznetsov, K. A. Birch, A. I. Boldyrev, X. Li, H. J. Zhai and L. S. Wang, *Science,* 2003, **300**, 622.

5 J. M. Mercero, M. Piris, J. M. Matxain, X. Lopez and J. M. Ugalde, *J. Am. Chem. Soc.,* 2009, **131**, 6949.

6 a) A. N. Alexandrova and A. I. Boldyrev, *J. Phys. Chem. A,* 2003, **107**, 554; b) D. Y. Zubarev and A. I. Boldyrev, *Phys. Chem. Chem. Phys.,* 2008, **10**, 5207.

7 I. A. Popov and A. I. Boldyrev in *The Chemical Bond. Chemical Bonding Across the Periodic Table*, *Vol. 14* (Eds. G. Frenking, S. Shaik), Wiley-VCH, 2014, pp 421.

8 E. Von Steuber, G. Elter, M. Noltemeyer, H. G. Schmidt and A. Meller, *Organometallics,* 2000, **19**, 5083.

9 a) E. Maslowsky, *Coord. Chem. Rev.,* 2011, **255**, 2746; b) S. Blanchard, L. Fensterbank, G. Gontard, E. Lacote, G. Maestri and M. Malacria, *Angew. Chem. Int. Ed. Engl.,* 2014, **53**, 1987; c) Y. Wang, A. Monfredini, P. A. Deyris, F. Blanchard, E. Derat, G. Maestri and M. Malacria, *Chem. Sci.,* 2017, **8**, 7394; d) C. Liu, N.V. Tkachenko, I.A. Popov, N. Fedik, X. Min, C. Q. Xu, J. Li, J. E. McGrady, A.I. Boldyrev and Z. M. Sun, *Angew. Chem. Int. Ed.,* 2019, **58**, 8367; e) N.V. Tkachenko, X.W. Zhang, L. Qiao, C.C. Shu, D. Steglenko, A. Munoz-Castro, Z.M. Sun and A.I. Boldyrev, *Chem. Eur. J.,* 2019, DOI: 10.1002/chem.201905264.

10 a) C. Liu, L. Li, I.A. Popov, R.J. Wilson, C. Xu, J. Li, A.I. Boldyrev, and Z.M. Sun, 2018, **36**, *Chin. J. Chem*., 1165; b) L. Li, B. Ali, Z. Chen, and Z.M. Sun. 2018, **36**, *Chin. J. Chem*., 955; c)X. Min, I. A. Popov, F. X. Pan, L. J. Li, E. Matito, Z. M. Sun, L. S. Wang and A. I. Boldyrev, *Angew. Chem. Int. Ed., Engl.* 2016, **55**, 5531.

11 a) E. Ruzin, A. Fuchs and S. Dehnen, *Chem. Commun.,* 2006, 4796; b) S. Scharfe and T. F. Fässler, *Eur. J. Inorg. Chem.,* 2010, 1207; c) Z. M. Sun, Y. F. Zhao, J. Li and L. S. Wang, *J. Cluster Sci.,* 2009, **20**, 601.

12 a) C. Downie, Z. J. Tang and A. M. Guloy, *Angew. Chem. Int. Ed.,* 2000, **39**, 338; b) T. F. Fässler and U. Schutz, *Inorg. Chem.,* 1999, **38**, 1866; c) A. Ugrinov and S. C. Sevov, *J. Am. Chem. Soc.,* 2002, **124**, 10990; d) A. Ugrinov and S. C. Sevov, *Inorg. Chem.,* 2003, **42**, 5789.

13 a) C. Schenk, F. Henke, G. Santiso-Quiñones, I. Krossing and A. Schnepf, *Dalton Trans.,* 2008, 4436. b) F. Li and S. C. Sevov, *Inorg. Chem.,* 2015, **54**, 8121. c) L.G. Perla, A. Muñoz-Castro, S.C. Sevov, *J. Am. Chem. Soc,* 2017, **139**, 15176.

14 R. J. Wilson, L. Broeckaert, F. Spitzer, F. Weigend and S. Dehnen, *Angew. Chem. Int. Ed. Engl.,* 2016, **55**, 11775.

15 S. Scharfe, T. F. Fässler, S. Stegmaier, S. D. Hoffmann and K. Ruhland, *Chem. Eur. J.,* 2008, **14**, 4479.

16 N. V. Tkachenko and A. I. Boldyrev, *Phys. Chem. Chem. Phys.,* 2019, **21**, 9590.

17 N. V. Tkachenko and A. I. Boldyrev, *Chem. Sci.*, 2019, **10**, 5761.

18 a) K. Wade, *Chem. Commun.*, 1971, **10**, 210; b) K. Wade, *Adv. Inorg. Chem. Radiochem.*, 1976, **16**, 1; c) D. M. P. Mingos, *Nat. Phys. Sci.*, 1972, **236**, 99.

19 a) F. Feixas, E. Matito, M. Duran, J. Poater and M. Solà, *Theor. Chem. Acc.,* 2010, **128**, 419; b) F. Feixas, E. Matito, J. Poater, M. Solà, *Chem. Soc. Rev.,* 2015, **44**, 6434.

20 R.F.W. Bader *Atoms in Molecules: A Quantum Theory*, Oxford University Press, Oxford, 1990.

21 M. Giambiagi, M.S. de Giambiagi, C.D. dos Santos Silva and A.P. de Figuereido, *Phys. Chem. Chem. Phys.,* 2000, **2**, 3381.

22 a) P. Bultinck, R. Ponec and S. Van Damme, *J. Phys. Org. Chem.,* 2005, **18**, 706; b) J. Cioslowski, E. Matito and M. Solà, *J. Phys. Chem. A,* 2007, **111**, 6521.

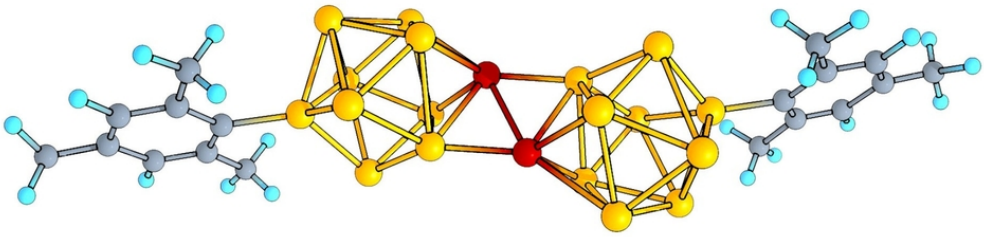

All-Metal σ-Antiaromatic Dimer

80x26mm (300 x 300 DPI)